Experimental studies of two-dimensional and three-dimensional structure in a crystallized dusty plasma

J. B. Pieper,[a] J. Goree,[b] and R. A. Quinn[c]
Department of Physics and Astronomy, The University of Iowa, Iowa City, Iowa 52242

(Received 4 October 1995; accepted 11 December 1995)

Coulomb crystallization of monodisperse 9.4-μm-diam spheres confined in a plasma is investigated in a modified GEC rf Reference Cell using various gases and electrode topographies. For some plasma conditions, planar electrodes confine particles radially in a few horizontal layers due to the curvature of the sheath boundary, and a two-dimensional (2D) hexagonal lattice is observed which structural analysis shows to be consistent with the intermediate ''hexatic'' phase of KTHNY 2D melting theory. A depression in the electrode surface causes a corresponding depression in the sheath and allows trapping of more layers in a three-dimensional (3D) structure, which is viewed in cross section by video imaging of a plane illuminated by a horizontal laser sheet. To synthesize 3D images, a stack of 2D images is made by moving the laser sheet and camera focal plane vertically through the particle cloud. This reveals regions of two stable 3D configurations within the cloud: body-centered-cubic and simple hexagonal with vertically aligned particles.

I. INTRODUCTION

The Coulomb crystallization of small particles in a plasma that has recently been observed[1–5] is significant both to condensed matter physics, where it shows promise of providing a new model system for studies of dynamics and phase transitions in solids, and to the investigation of strongly coupled interactions between plasma components, including those involving dust grains. The crystallization is enabled by the high negative charge acquired by the particles due to the electron and ion fluxes at the particle surface.[6,7] The particles interact strongly by a screened Coulomb potential and form a regularly ordered array if their size dispersion, and hence their charge dispersion, is small. There also must be a suitable confining force to hold the system of particles together against the electrostatic repulsion. The crystallization therefore is strongly influenced by the electric potential inside the containing vessel. Particles are levitated by a vertical electric field in a sheath, which balances the downward forces of gravity and ion drag. If the lower electrode is not flat, its topographical features can produce traps for the particles.[8] In the horizontal direction particles are trapped by the sheath curvature. They tend to arrange themselves into multiple horizontal layers, with the lower layers occupied by heavier particles. The pattern is chiefly two-dimensional (2D) when only a few layers are present. When there are many layers, however, interaction between layers becomes important and three-dimensional (3D) ordered structures can be discerned.[9] The effective dimensionality of the crystal, and perhaps the types of structures formed, are sensitive to the details of the trapping potential. For example, a deeper potential well can trap more particles in more horizontal layers than a shallow well.

[a]Electronic mail: pieper@dusty.physics.uiowa.edu
[b]Electronic mail: john-goree@uiowa.edu
[c]Electronic mail: quinn@iowa.physics.uiowa.edu

We report here studies of the crystal structures formed by monodisperse polymer particles of 9.4 μm diameter, in a rf plasma reactor for various gases and electrode topographies. We find that the radial trapping potential that forms above a planar electrode generally is sufficient to hold a few layers of particles in a 2D hexagonal lattice, although this does depend to some extent on the gas species and pressure. By altering the electrode surface topography, the trap can be altered to hold a larger number of stacked planes of particles; this promotes the formation of 3D ordered structures. We also report a method of obtaining direct images of the 3D crystal structures in which both the horizontal and vertical positions of the particles are resolved.

II. EXPERIMENTAL TECHNIQUES

The experiments were conducted in a Gaseous Electronics Conference (GEC) rf Reference Cell.[10] For this application, the upper of the two 4-in.-diam Al electrodes was removed and an optical window was installed above its location, in the electrode port, for imaging the dust crystal. The lower electrode was capacitively coupled to the rf amplifier through a π-type matching network. The reactor walls served as the ground return. The electrode rested upon a Teflon insulator that was covered by a ground shield.

The experimental setup is shown schematically in Fig. 1. The particle cloud was imaged using horizontal and vertical sheets of laser light and a pair of high-resolution charge coupled device (CCD) video cameras, one mounted above the top window and one at a side window. Most of our images, including all those shown here, are made using the horizontal laser sheet and the top camera, which was connected to a video recorder and a frame grabber. To attain a highly uniform brightness, the horizontal sheet was formed by a rotating polygonal mirror (Lincoln Laser model DT-24-252-037) that has 24 facets and turns at 8200 rpm. It swept a He–Ne laser beam that was focused to a Gaussian half-width

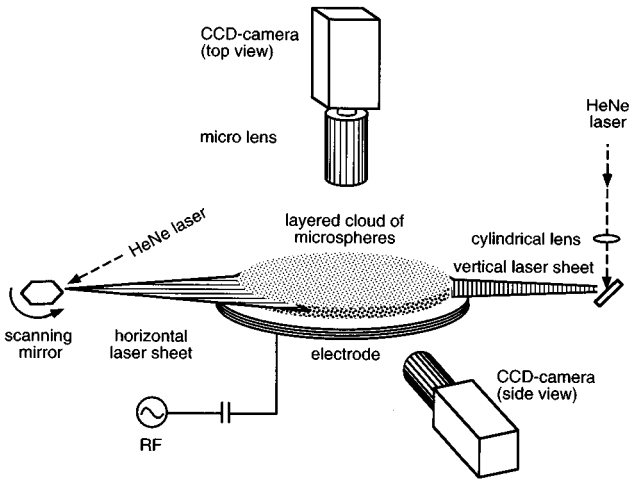

FIG. 1. Schematic of experimental setup. A discharge is created above the electrode by applying a rf voltage between it and the surrounding vacuum chamber (not shown). Charged microspheres are levitated ~2 mm above the electrode. Laser sheets and video cameras allow viewing of the dust cloud from the top and side.

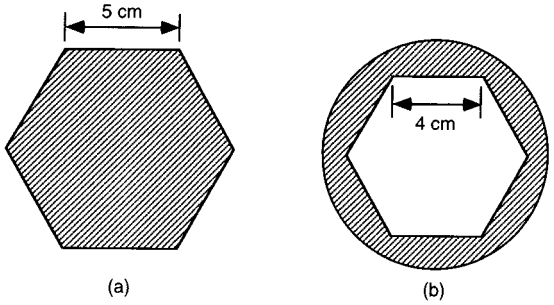

FIG. 2. Electrode plates made from 1.5-mm-thick Al sheet: (a) solid hexagonal, (b) hexagonal cutout.

of 45 μm in the imaged volume. The mirror was tilted to align the light sheet with the horizontal planes of particles. In comparison to the rotating mirror, other methods of producing laser sheets yield a less uniform brightness. A cylindrical lens, such as that we use for the vertical sheet, produces an expanded beam containing all the spatial mode structure or Gaussian profile of the incoming beam. A galvanometer laser scanner uses a mirror that sweeps back and forth in an angle less than a full circle, coming to a rest at each extreme. Its acceleration causes the laser sheet to be dimmest at its center and brightest near its edges.

For imaging of three-dimensional structures, the heights of the laser optics and the camera were controlled by lead screws turned by stepping motors. The two were moved together in the vertical direction, keeping the camera in focus with the laser sheet. A programmable motor controller set their heights with a resolution of 5 μm. The height was measured from the voltage output of a linear potentiometer that was mechanically coupled to the translating laser optics. We typically started a run at the top of the particle cloud and lowered the imaging plane in 30 μm steps, pausing for one second at each step, while recording the images on the video recorder. Depending on the cloud thickness, 20–30 image layers were recorded in this way. Since the step size was less than the beam full-width of 90 μm, the volume imaged at each height overlapped with the next. Thus, none of the particles could be missed.

Three-dimensional images of the crystal structure were synthesized by interpolating brightness data between the heights of the 2D video image planes. The resolution was greatest in the horizontal direction; in the vertical direction it was limited by the laser beam width. Since the images for each height were taken at different times, it was necessary to correct for a small secular drift of the whole particle cloud. The drift velocity was typically a few tens of μm/s. During the 1 s delay between consecutive images, particles moved less than half their average separation, and most of the drift error could be easily corrected. This correction was done by exploiting the vertical overlap between image volumes, which meant that the same particle could be identified in two consecutive planes. A plane was shifted horizontally so that in both planes a given particle appeared at the same horizontal coordinates. Once this was done for a single particle, all the particles in the images were well aligned. This was repeated for each consecutive pair of planes.

The particles used were monodisperse polymethylene melamine spheres of density 1.514 g/cm^3 and diameter (and dispersion) of 9.4 ($\pm$ 0.3) μm. They were introduced into the glow region of the plasma from a dispenser with an opening covered with a fine-wire mesh. The dispenser was withdrawn from the electrode region after the particles were shaken out. All observations of the particles were made with no gas flow.

Two different electrode surfaces were fabricated from Al sheet stock and placed on top of the original Al electrode. The first was a solid plate cut in the shape of a hexagon with each side being 5 cm, Fig. 2(a), and the second was a disk equal in diameter to the original electrode, with a hexagon of 4 cm sides cut out of the center, Fig. 2(b). The hexagonal shape was chosen to determine if it would influence the formation of the crystal by providing boundary conditions appropriate to the typically hexagonal lattice. Its orientation turned out to have little or no effect on the orientation of the lattice except in the cloud's periphery at the edge of the hexagon, where the particles tended to align parallel to the edge. The cutout and disk plates were both 1.5 mm thick. If the cutout plate had been much thicker, particles would have been levitated below the height of its rim, and it would have been impossible to illuminate them from the side.

The GEC Reference Cell was electrically characterized as recommended in Ref. 10 to measure the rf power dissipated in the discharge. We estimated the plasma density by measuring the ion saturation current collected by a cylindrical Langmuir probe 0.127 mm in diameter and 8.0 mm long, biased up to 80 V below the plasma potential, and interpreting the result using Allen–Boyd–Reynolds (ABR) theory[11,12] for the ion current and an estimated electron temperature of $kT_e = 3.0 \pm 0.5$ eV.

III. TEST RESULTS

Generally, when the flat hexagonal plate was installed on the electrode, particles were trapped above it on an equipotential surface. Three or four layers of particles (as determined by side viewing) would typically spread out to cover about two-thirds of the area above the plate. Additional particles that were at the large end of the size distribution and aggregates of two or more particles would accumulate over the center of the electrode, below the full layers. A number of lighter particles would also appear in the center region above the full layers, giving the cloud a domelike shape. Adding more particles would temporarily increase the number of layers, but particles would gradually escape from the edge of the cloud on a time scale of tens of minutes until there were once again three or four layers.

The trapping was sensitive to the gas pressure and to the rf power. For all the inert gases except helium, below a certain critical pressure particles escaped rapidly (on time scales of seconds to minutes) at higher powers, while above the critical pressure trapping was stable at all available powers. For the neon discharge the critical pressure was about 3 Torr, but it was much smaller for the heavier gases: about 1.0, 0.9, and 0.8 Torr for Ar, Kr, and Xe, respectively. With helium the situation was reversed: at 0.5 Torr the particles were stably trapped at all rf power levels, but above about 0.8 Torr the cloud became ring shaped, and at powers of 2 W or more the ring expanded nearly to the electrode diameter and the particles escaped. The explanation for this is not known, but it is likely that the potential profile above the electrode depends on the gas species and pressure.

With the cutout electrode plate in place, a depression in the plasma–sheath boundary was clearly visible above the cutout area. When a sufficient number of particles was introduced above this electrode surface, the resulting cloud would expand and completely fill the area of the depression. The cutout plate resulted in a significantly more uniformly planar particle cloud than that above the flat electrode, confined particles over a wider range of pressure and power, and permitted the trapping of a much larger number of layers, which is needed for the formation of extended 3D structures. Heavy particles and aggregates again accumulated in or below the lowest layer. These large grains caused perturbations leading to disorder in the planes above them, in the main part of the cloud. To reduce this problem, we removed most of the large grains from the cloud by decreasing the rf power until the heaviest particles fell to the electrode, while we viewed from the side. Then the power was increased again to the desired operating point.

The conditions of power and gas pressure that produced the most ordered arrangement of particles varied with the gas species. Generally, high pressures were more favorable, and the required pressure for high ordering varied inversely with the atomic weight of the gas, which is expected since the particles are cooled by collisions with nearly room-temperature neutral gas atoms, and collisions redistribute kinetic energy between the particles and the neutrals more effectively if the neutral atoms are more massive. We used one of the heavier gases (Kr) in the crystallization experiments to take advantage of this more effective cooling.

In each experiment there was an optimum discharge power that produced the most ordered structure. At low power the plasma density is reduced and the Debye length and correspondingly the average particle separation are increased. This seems to reduce the interparticle interaction. At high power the particle kinetic energy is increased, presumably due to low-frequency fluctuations in the local electric field.[13] The cause of the low-frequency fluctuations has not been identified, but may be ion acoustic instabilities in the sheath or fluctuations in the ionization balance.

IV. IMAGING OF THE COULOMB SOLID

We present an image of particles in a 2D hexagonal lattice in Fig. 3. The electrode was fitted with the solid hexagonal electrode plate, shown in Fig. 2(a), and the plasma was operated with Kr at 1.3 Torr. The rf power was 2.0 W, with a voltage of 105 V p–p at the electrode and a -50 V dc self-bias. The plasma density was $\sim 6\times 10^8$ cm^{-3} in the brightest part of the glow, about 2 mm above the electrode. The particle cloud was three to four layers thick. The highest layer is shown in Fig. 3. Particles in the lower layers were aligned vertically with those shown. This vertical coupling of the particles with few layers seems to make the entire cloud well characterized as a 2D structure. The average particle spacing Δ is 128 ± 1 μm. Figure 3(b) is the Voronoi diagram obtained from the image, which confirms its hexagonal character. Over 98% of the Voronoi cells are six-sided, and the defects, which are marked on the diagram, are nearly all free dislocations consisting of a tightly bound pair of five- and sevenfold-coordinated particles. Figure 4 shows plots of the pair correlation function $g(r)$ and the bond-orientation correlation function $g_6(r)$ for this crystal, calculated as described in Ref. 14. The data are fit by exponentially decaying functions, yielding correlation lengths $\xi = (7.4 \pm 0.8)\,\Delta$ for $g(r)$ and $\xi_6 = (128 \pm 10)\,\Delta$ for $g_6(r)$. We also fit g_6 by a power-law decay, obtaining a decay exponent η of 0.038 ± 0.002.

The KTHNY theory of two-dimensional phase transitions[15–17] predicts that a crystal melts into a so-called hexatic phase, which melts gradually into an isotropic liquid phase. For the structure of Fig. 3, the range of orientational order is much longer than that of translational order ($\xi_6 \geqslant \xi$) the power law exponent falls in the range $0 < \eta < 0.25$, and free dislocations are present. These three observations are consistent with identifying the phase as hexatic, according to the KTHNY theory.

Colloidal experimenters[18] offer additional empirical criteria for their 2D experiments, which might be applied to our image for a dusty plasma. Images they identified as hexatic were characterized by $0.05 \leqslant \eta \leqslant 0.25$ and $4 < \xi/\Delta < 18$. The values for Fig. 4 of $\eta = 0.038$ and $\xi/\Delta = 7.4$ are roughly consistent with this identification of the hexatic phase. The structures they identified as a crystal near melting were 95% sixfold coordinated and contained no defects other than pairs

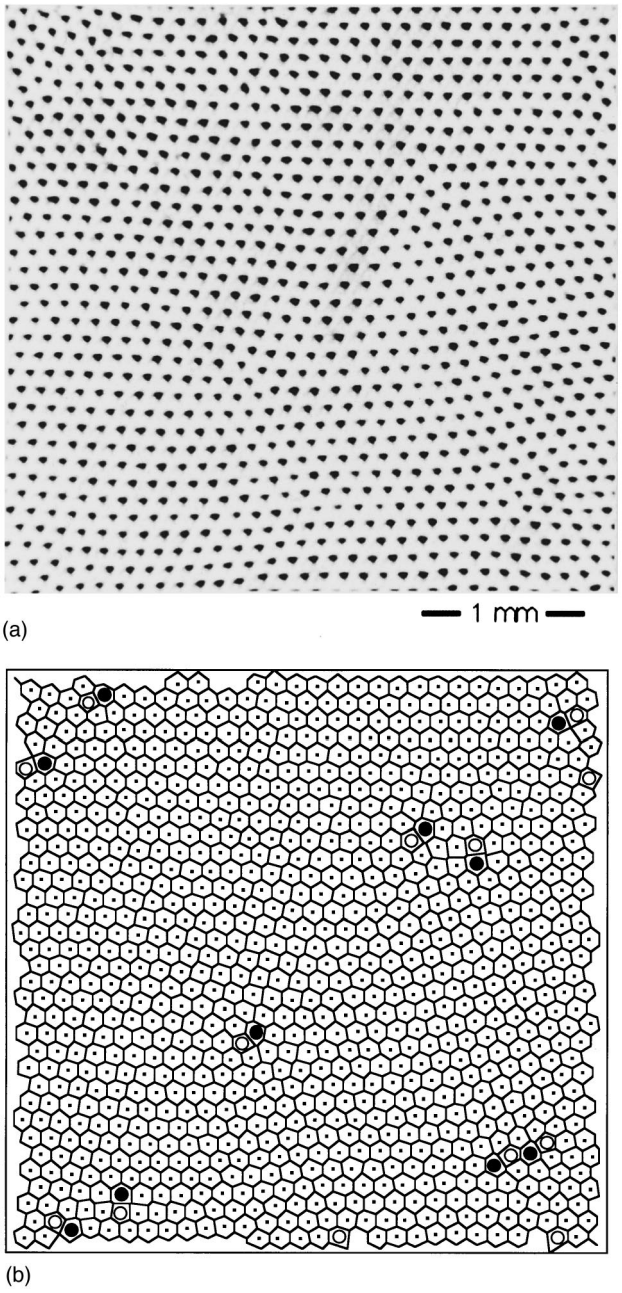

FIG. 3. (a) Brightness-inverted image of the 2D hexagonal lattice formed by 9.4-μm-diam polymer spheres in a 1.3 Torr Kr discharge above the electrode of Fig. 2(a). (b) Voronoi diagram of the image in (a). The particles are labeled according to their number of nearest neighbors (coordination number) as follows: (○) 5, (•) 6, (●) 7.

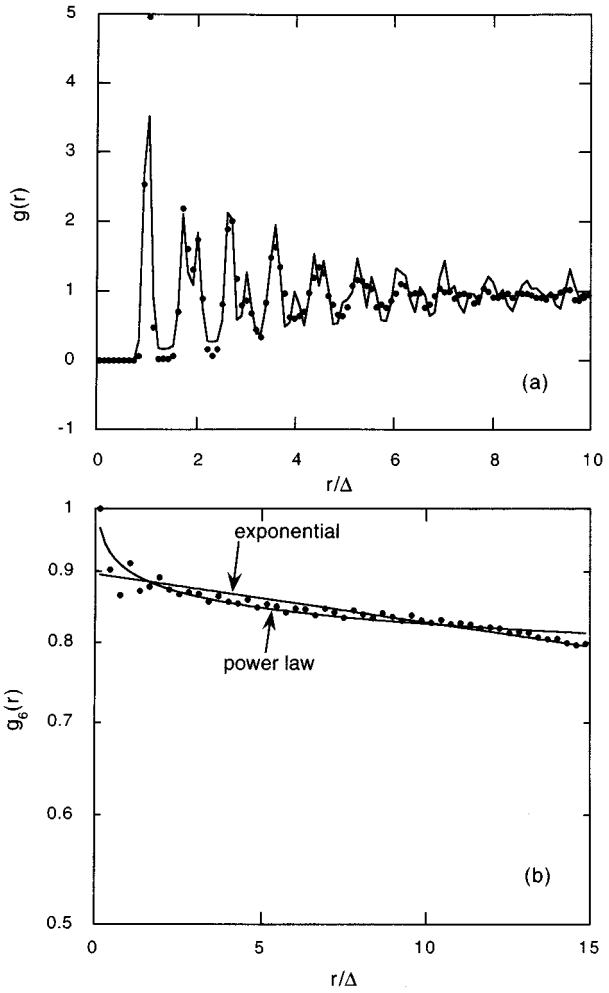

FIG. 4. (a) The pair correlation function $g(r)$ for the 2D crystal pictured in Fig. 3. The data are fit by a series of Gaussian peaks with the correct relative positions and heights for a hexagonal crystal, multiplied by a decaying exponential envelope. The exponential scale factor, identified as the correlation length ξ, has a fit value (7.4 ± 0.8) Δ. (b) The bond-orientation correlation function $g_6(r)$ for the 2D crystal, fit by exponential and power-law decays. The fit values are (125 ± 10) Δ for the exponential correlation length ξ_6 and 0.038 ± 0.002 for the power-law exponent η. Error bars for the data points in both plots are approximately the size of the data point symbols.

and triplets; according to this, the image shown in Fig. 3 would be near the melting transition on either the crystalline or hexatic side.

An example of a three-dimensional structure is shown in Fig. 5. The brightness values (in arbitrary units as measured by the frame grabber) are computed everywhere in the sample volume by using linear interpolation between the image planes. The software produces an image of the data in an arbitrarily oriented plane within the sample volume. The structure pictured was observed with the cutout plate of Fig. 2(b) on the electrode in a 1.4 Torr Kr discharge at 2.3 W rf power (180 V p–p at the electrode, −43 V dc self-bias), with an estimated plasma density in the glow 2 mm above the electrode of 6×10^8 cm^{-3}. In this case the particles were found to be arranged on a square lattice in the horizontal plane, as shown in the inset. Particles in adjacent planes are dimly visible, being slightly illuminated by the edge of the laser beam; these are also on a square lattice with the lattice points in the center of the squares of the brightly illuminated plane. This pattern repeats as we step down vertically through the cloud, and persists through its entire thickness, with about ten lattice planes resolvable. The structure is therefore that of either a body-centered-cubic (bcc) or face-centered-cubic (fcc) lattice in three dimensions, with a ⟨100⟩ axis in the vertical direction. The main part of Fig. 5 shows the outline of the volume covered by the data set, with one

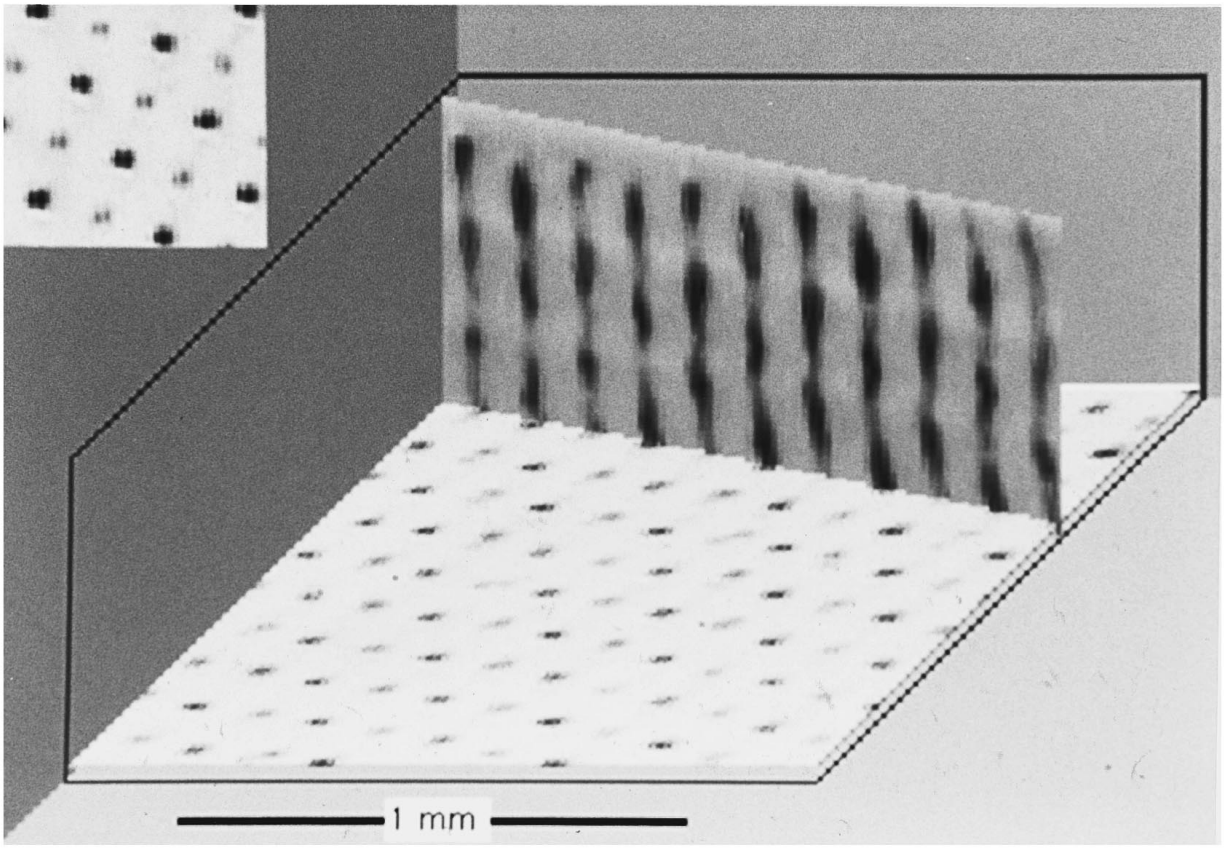

FIG. 5. One horizontal plane and a vertical cross section showing a 3D bcc structure formed by 9.4-μm-diam polymer spheres in a 1.4 Torr Kr discharge above the electrode of Fig. 2(b). The inset shows a portion of the horizontal plane viewed from above. The brightness data is inverted. The 3D image consists of a stack of horizontal planar images resolved by selective illumination by a 90-μm-thick sheet of light from a focused, swept laser beam. The vertical cross section is taken along a {110} plane of the bcc lattice. In the vertical plane the particle images appear longer in the vertical direction due to the finite thickness of the laser sheet.

image of a horizontal lattice plane and a vertical slice taken along a diagonal of squares in the horizontal plane. The particle spacing in the horizontal {100} planes is 194 $\pm$ 1 μm, and the mean distance between the planes is 100 $\pm$ 20 μm. This last number should be compared with the expected plane spacings of 97 and 137 μm for the bcc and fcc structures, respectively, given the measured in-plane particle spacing. The data is more consistent with the bcc structure, and we identify the vertical slice in Fig. 5 as being along a {110} plane. We show a sketch of the bcc structure, which may be compared with the data in Fig. 6. Further analysis of the observed bcc crystal will be presented elsewhere.[19]

In addition to the bcc structure, we observed elsewhere in the same dust cloud a different configuration known as the ''simple hexagonal'' structure. In it, particles are arranged in a hexagonal lattice in the horizontal plane and are aligned vertically, one directly above the next. We observed a plane separation equal to the in-plane particle spacing (within the precision of the vertical particle coordinates). Regions of the simple hexagonal and bcc structures coexisted in neighboring parts of the cloud, and had the same in-plane spacing (to within measurement error). Figure 6(b) is a sketch of this structure. Although it is commonly observed in plasma dust crystals,[9,20] it is not a minimum-energy configuration of particles if the repulsive screened-Coulomb potential is considered alone. The possibility of an additional attractive potential arising from collective interactions involving the ion flow toward the electrode has recently been shown,[21–23] and could be responsible for its appearance as a stable configuration.

V. CONCLUSIONS

We have observed highly ordered structures in Coulomb crystals of 9-μm-diam particles in a rf plasma, including one

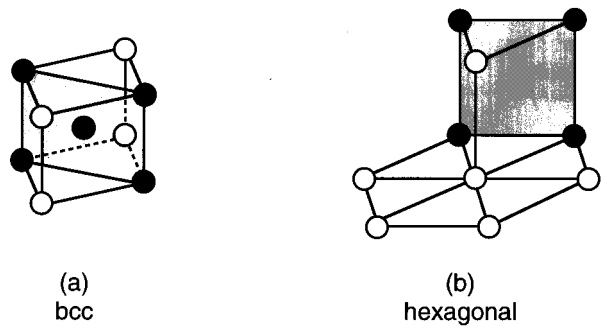

FIG. 6. Sketches of the bcc and hexagonal unit cells. The bcc cell is aligned as in Fig. 5; its {110} plane is shown shaded.

that two-dimensional analysis shows to be consistent with the hexatic phase of the 2D KTHNY theory. The particle trapping necessary for formation of the structures depends on the gas species and pressure as well as electrode topography. Under favorable conditions the particle configuration extends far enough vertically for three-dimensional structures to be identified, and imaged directly in 3D by selective illumination. The 3D images reveal the presence of lattice structures such as the body-centered-cubic.

ACKNOWLEDGMENTS

This work was supported by NASA and by the National Science Foundation (NSF). The authors thank D. Dubin, A. Piel, and H. Thomas for helpful discussions.

[1]H. Thomas *et al.*, Phys. Rev. Lett. **73**, 652 (1994).
[2]J. H. Chu and Lin I, Phys. A **205**, 183 (1994).
[3]Y. Hayashi and K. Tachibana, Jpn. J. Appl. Phys. **33**, 804 (1994).
[4]A. Melzer, T. Trottenberg, and A. Piel, Phys. Lett. A **191**, 301 (1994).
[5]T. Trottenberg, A. Melzer, and A. Piel, Plasma Sources Sci. Technol. **4**, 450 (1995).
[6]J. Goree, Plasma Sources Sci. Technol. **3**, 400 (1994).
[7]J. Goree, IEEE Trans. Plasma Sci. (submitted).
[8]G. S. Selwyn, J. E. Heidenreich, and K. L. Haller, Appl. Phys. Lett. **57**, 1876 (1990).
[9]J. H. Chu and Lin I, Phys. Rev. Lett. **72**, 4009 (1994).
[10]P. J. Hargis, Jr. *et al.*, Rev. Sci. Instrum. **65**, 140 (1994).
[11]J. E. Allen, R. L. F. Boyd, and P. Reynolds, Proc. Phys. Soc. London Sect. B **70**, 297 (1957).
[12]F. F. Chen, Plasma Phys. **7**, 47 (1965).
[13]J. H. Chu, J.-B. Du, and Lin I, J. Phys. D **27**, 296 (1994).
[14]R. A. Quinn *et al.*, Phys. Rev. E (in press).
[15]J. M. Kosterlitz and D. J. Thouless, J. Phys. C **6**, 1181 (1973).
[16]B. I. Halperin and D. R. Nelson, Phys. Rev. Lett. **41**, 121 (1978).
[17]A. P. Young, Phys. Rev. B **19**, 1855 (1979).
[18]C. A. Murray, W. O. Sprenger, and R. A. Wenk, Phys. Rev. B **42**, 688 (1990).
[19]J. B. Pieper, J. Goree, and R. A. Quinn, Phys. Rev. Lett. (submitted).
[20]A. Melzer, A. Homann, and A. Piel, Phys. Rev. E (submitted).
[21]S. V. Vladimirov and M. Nambu, Phys. Rev. E **52**, R2172 (1995).
[22]F. Melandsø and J. Goree, Phys. Rev. E **52**, 5312 (1995).
[23]F. Melandsø and J. Goree, J. Vac. Sci. Technol. A **14**, 511 (1996).